

1 **Measurement report: On the contribution of long-distance transport to the secondary**
2 **aerosol formation and aging**

3 Haobin Zhong^{1,2}, Ru-Jin Huang^{1,2,3}, Chunshui Lin¹, Wei Xu¹, Jing Duan¹, Yifang Gu^{1,2}, Wei
4 Huang¹, Haiyan Ni¹, Chongshu Zhu¹, Yan You⁴, Yunfei Wu⁵, Renjian Zhang⁵, Jurgita
5 Ovadnevaite⁶, Darius Ceburnis⁶, Colin D. O'Dowd⁶

6 ¹State Key Laboratory of Loess and Quaternary Geology (SKLLQG), Center for Excellence in
7 Quaternary Science and Global Change, and Key Laboratory of Aerosol Chemistry and Physics,
8 Institute of Earth Environment, Chinese Academy of Sciences, Xi'an 710061, China

9 ²University of Chinese Academy of Sciences, Beijing 100049, China

10 ³Open Studio for Oceanic-Continental Climate and Environment Changes, Pilot National
11 Laboratory for Marine Science and Technology (Qingdao), 266061 Qingdao, China

12 ⁴National Observation and Research Station of Coastal Ecological Environments in Macao,
13 Macao Environmental Research Institute, Macau University of Science and Technology, Macao
14 SAR 999078, China

15 ⁵Key Laboratory of Middle Atmosphere and Global Environment Observation (LAGEO),
16 Institute of Atmospheric Physics, Chinese Academy of Sciences, Beijing 100029, China

17 ⁶School of Physics and Ryan Institute's Centre for Climate & Air Pollution Studies, National
18 University of Ireland Galway, University Road, Galway H91CF50, Ireland

19
20 Correspondence to: Ru-Jin Huang (rujin.huang@ieecas.cn)

21
22 **Abstract**

23 To investigate the physio-chemical properties of aerosol transported from major pollution regions
24 in China, observations were conducted ~200 m above the ground at the junction location of the
25 North China Plain and Fenwei Basin, which are two regions of top priority for China's blue sky
26 campaign. We identified three pollution transport sectors including those from Beijing-Tianjin-
27 Hebei (BTH), urban Guanzhong Basin (GZB), northern China and one clean transport sector from
28 rural Guanzhong Basin region. Secondary inorganic aerosol (SIA) constituted a major fraction (39-
29 46%) in all pollution transport sectors with high sulphur oxidation ratio (0.44-0.58) and nitrogen
30 oxidation ratio (0.24-0.29), suggesting efficient formation of secondary inorganic aerosol during
31 regional transport. While more oxidized oxygenated organic aerosol (MO-OOA) played a dominant
32 role **in the source of organic aerosol** in all sectors including the clean one, accounting for 42-58%
33 of total organic aerosol. Elemental analysis (O and C) shows that aerosol particles at this receptor
34 site were much more oxidized than urban regions, pointing that long-range transport contributed
35 markedly to the organic aerosol oxidation and aging. Case studies of pollution events with high
36 sulphate, nitrate and more-oxidized oxygenated organic aerosol production rate indicate the strong
37 formation efficiency of secondary aerosol during regional transport in the Beijing-Tianjin-Hebei

38 transport sector.

39 **Keywords:** Regional transport; Secondary aerosol formation; More oxidized organic aerosol;
40 Air pollution.

41 **1 Introduction**

42 Air pollution events with high levels of fine particles (particulate matter with a diameter ≤ 2.5
43 μm , $\text{PM}_{2.5}$) were frequently occurred in China over the past years, due to rapid industrialization
44 and urbanization (Lelieveld et al., 2015; Feng et al., 2018; An et al., 2019). The high level of
45 $\text{PM}_{2.5}$ affects air quality, human health and climate, thus, has received widespread concerns
46 around the world (Tie et al., 2016; Cohen et al., 2017). To better understand air pollution in
47 China, many field studies has been carried out in the last decades (Tie et al., 2009; Lei et al.,
48 2011; Cao et al., 2012; Huang et al., 2014; [Liu et al., 2018](#)). Most of these studies for particle
49 properties are based on local observations, such as in Beijing (Sun et al., 2013; Li et al., 2019),
50 Shanghai (Xu et al., 2012; Huang et al., 2013; Wang et al., 2020), Xi'an (Huang et al., 2014;
51 Duan et al., 2021; Lin et al., 2022), Guangzhou (Guo et al., 2020; Chen et al., 2021), and Hong
52 Kong (Li et al., 2015; Sun et al., 2016). However, aerosol particles can affect hundreds of
53 kilometers through transport depending on particle size and chemical compositions (Uno et al.,
54 2009). During transport, aerosols undergo further transformation, altering chemical
55 composition and oxidation level and consequently affecting their chemo-physical properties
56 and climate impact (Moffet and Prather, 2009; Riemer and West, 2013; Calvo et al., 2013;
57 Fierce et al., 2016).

58 Recent studies found that local formation cannot fully explain the increase of SIA during
59 pollution events, and the regional transport was considered as an important source for the
60 increase of SIA (Yang et al., 2015; Tang et al., 2016). Some modeling studies reported that
61 heterogeneous chemistry during the transport was identified as the dominant factor during haze
62 episodes in mega cities (Li and Han, 2016; Li et al., 2017), and were further supported by the
63 observations. Du et al. (2019) reported that the chemical transformation from SO_2 to sulphate
64 was the major source of sulphate in Beijing. Li et al. (2021) suggested that the pollution in
65 winter in Beijing was largely affected by the regional transport, and the water vapor during the
66 transport of the air mass greatly increased SIA proportion. Gunsch et al. (2018) claimed that
67 the particles were heavily coated with SOA formed during the transport, with 89% of organics
68 fractions in PM_1 and 0.8 O/C ratio in the forested Great Lakes region during wild-fire period.
69 Most of the existing studies were devoted to studying the contribution of regional transport to
70 pollution events in urban areas, while the study on region-to-region transport was limited. Our
71 previous study reported that different regions in China represented different chemical
72 compositions and OA sources due to different types of emission characteristics (Zhong et al.,
73 2020). Therefore, the transport aerosol particles from different regions may have completely
74 different properties due to different precursors and transport conditions. The study of region-
75 to-region transport can provide insight to the interactions and mixing properties of particles on
76 a national scale.

77 Investigation of the chemical compositions and sources with the transport pathways in
78 background areas is a common method to understand the influence of long-distance transport

79 of aerosol on the atmospheric environment (Schichtel et al., 2006; Salvador et al., 2008; Das
80 and Jayaraman, 2012; Tang et al., 2014; Pu et al., 2015). In this study, we performed a ~~two-~~
81 ~~months~~one-month observation at a regional receptor site to investigate the characteristics of
82 aerosol transported from the major pollution regions by using a time-of-flight aerosol chemical
83 speciation monitor (TOF-ACSM). The receptor site is geographically located in the middle part
84 of China, at the junction of the BTH region and the GZB region, which are the two of the three
85 key regions in Protection of Blue Sky issued by the National Congress for pollution control and
86 sustainable development in 2018. In addition, the chemical composition of non-refractory PM_{2.5}
87 (organics, sulphate, nitrate, ammonium, and chloride) and OA source apportionment were
88 resolved and analyzed with measured black carbon, gas-phase pollutants (SO₂, CO, NO₂ and
89 O₃) and meteorological parameters to provide complementary mass-based characterization of
90 the transported aerosols.

91 **2 Experimental**

92 **2.1 Sampling site and instrumentation**

93 The sampling was carried out on the rooftop of Le Méridien hotel, which was a 33-floor tall
94 building and about 200 meter above the ground (34.34°N, 109.02°E), during summer from 19th
95 May to 18th June 2018. It is located in the central area of Chan-ba Ecological District (CBE,
96 129 km²), which was a new ecological district, located at the eastern part of the GZB region.
97 The sampling site was surrounded by wetlands and lawns.

98 A TOF-ACSM (Aerodyne Research Inc., Billerica, MA) was deployed in an air-conditioned
99 room on the top floor (32nd) of Le Méridien hotel for continuous on-line measurements of non-
100 refractory PM_{2.5} species including organics (Org), sulphate (SO₄²⁻), nitrate (NO₃⁻), ammonium
101 (NH₄⁺), and chloride (Cl⁻). The sampling time resolution was 5 minutes. Also, a scanning
102 mobility particles sizer with a differential mobility analyzer (SMPSDMA, model 3080) and a
103 condensation particle counter (CPC, model 3772) (TSI Incorporated, Shoreview, Minnesota,
104 USA) were combined for the particle number size distribution measurement between 10 ~ 840
105 nm, which shared an inlet with TOF-ACSM through a PM_{2.5} cyclone (URG-2000-30ED, URG
106 Corp., Chapel Hill, NC). Black carbon concentration was measured by an aethalometer (AE33,
107 Magee Scientific) through an individual PM_{2.5} cyclone (SCC, BGI) inlet. The sampling time-
108 resolution was 1 min at a flow rate of 5 L min⁻¹. Gas-phase pollutants (SO₂, CO, NO, NO₂ and
109 O₃) were measured by the gas analyzers (Thermo Scientific Inc.). Meteorological data
110 (temperature, RH, wind speed and wind direction) were measured by an automatic weather
111 station (MAWS201, Vaisala, Vantaa, Finland) and a wind sensor (Vaisala Model QMW101-
112 M2). All ambient inlets of instruments were set on the rooftop (33rd, 200 m) and were 1.5 m in
113 height.

114 **2.2 TOF-ACSM operation**

115 TOF-ACSM has been detailed previously (Fröhlich et al., 2013). Briefly, ambient air was
116 sampled through a PM_{2.5} cyclone and a 3/8-inch polished stainless-steel tube (Swagelok
117 company, Solon, OH) with a constant flow rate of 3 L min⁻¹ (0.3 L min⁻¹ for SMPS and CPC,
118 0.08 L min⁻¹ for TOF-ACSM and 2.62 L min⁻¹ for an extra constant flow air pump) for the

119 coarse particles cut. Following that, particles were focused into a narrow particle beam via a
120 PM_{2.5} aerodynamic lens. Then the particles were evaporated by a thermal standard vaporizer (~
121 600°C) and ionized by an electron impact ionization (70eV), and the resulting ion fragments
122 were analyzed and determined by a time-of-flight mass spectrometer. Also, a Nafion dryer was
123 used to remove moisture prior to entering TOF-ACSM and SMPS, which kept the relative
124 humidity (RH) of the particle beam under 30%. Meanwhile, an automatically switching valve
125 was installed on the main air path between the Nafion dryer and TOF-ACSM, which was set to
126 change the sampling flow to a high-efficiency particulate air filter for the detection limits
127 measurement during the acquisition.

128 Ionization efficiency (IE) and relative ionization efficiency (RIE) calibrations were performed
129 about every ~10 days during the campaign. Briefly, pure ammonium nitrate and ammonium
130 sulphate particles were successively atomized by a TSI 3076 atomizer (TSI Incorporated,
131 Shoreview, Minnesota, USA). After that, they were dried by a hollow silica gel drying tube
132 before being imported into SMPS for 300 nm size selection, and then were counted and
133 measured by CPC and TOF-ACSM simultaneously. The other parameter calibrations, such as
134 the mass, the baseline, and the single ions were conducted every 3 days.

135 **2.3 Data analysis**

136 The chemical compositions and mass concentrations of PM_{2.5} were analyzed by Tofware
137 (v2.5.13, Tofwerk AG). Organics, nitrate and chloride were analyzed with RIEs of 1.4, 1.1 and
138 1.3, respectively (Canagaratna et al., 2007). RIEs of ammonium and sulphate were estimated
139 from the averaged results of IE and RIE calibration (4.7 for RIE of ammonium; 0.67 for RIE of
140 sulphate). Besides, a particle collection efficiency (CE) for particle bounce losses was
141 calculated as a value of 0.5, with a slight adjustment of CE value was based on a composition
142 dependent collection efficiency (CDCE) approach following Middlebrook et al., 2012. The
143 resulting mass concentrations of chemicals of PM_{2.5} were well correlated with the mass
144 concentrations of water-soluble inorganic aerosol from our In-situ Gas and Aerosol
145 Compositions monitor (IGAC, S-611, MachineShop) measurement (Fig. S2), suggesting the
146 reliability of TOF-ACSM results analysis.

147 The OA source apportionment was performed by positive matrix factorization (PMF, Paatero
148 and Tapper, 1994; Paatero, 1997) and multilinear engine (ME-2, Paatero, 1999). Organic
149 aerosol matrices (data matrix, error matrix, minimum values, time series and m/z from ~~412~~~120
150 ~~amu~~–~~amus~~ in our case) were exported from Tofware, and were resolved for source
151 apportionment in PMF-ME-2 Toolkit SoFi (version 6.3, Canonaco et al, 2013). The optimal
152 factor-selection and constraining strategies of SoFi were described by Elser et al. (2016). The
153 details are presented in section S1 of the supplementary.

154 **2.4 Trajectory analysis**

155 The trajectory analysis was performed using the HYSPLIT model (Draxler and Hess, 1998) in
156 Hybrid Single-Particle Lagrangian Integrated Trajectory (HYSPLIT_4). Briefly, trajectories
157 were calculated every one hour from the air mass data which were downloaded from the
158 National Oceanic and Atmospheric Administration (NOAA,

159 ftp://arlftp.arlhq.noaa.gov/pub/archives/gdas1) with 48 hours backward at a height of 200 m.
160 The trajectories were further clustered using in TrajStat (TrajStat_v1.2).

161 2.5 Sulphur oxidation ratio and nitrate oxidation ratio

162 Sulphur oxidation ratio (SOR) and nitrate oxidation ratio (NOR) are the ratios of sulphate and
163 nitrate to their gaseous precursors, which were widely used to represent the degree of gas-to-
164 particle conversions of sulphur and nitrogen. SOR and NOR are calculated by solving Eq. (1)
165 and (2) (Ji et al., 2018; Chang et al., 2020).

$$166 \text{ SOR} = n[\text{SO}_4^{2-}]/(n[\text{SO}_4^{2-}] + n[\text{SO}_2]) \quad (1)$$

$$167 \text{ NOR} = n[\text{NO}_3^-]/(n[\text{NO}_3^-] + n[\text{NO}_2]) \quad (2)$$

168 3 Results and discussion

169 3.1 Overview of the chemical composition, OA sources and regional transport in the 170 receptor site

171 The observational site with an altitude of ~200m above the ground provides ideal to investigate
172 the impact of regional transport on aerosol properties. Figure 1 shows an overview of the time
173 series of the chemical components of NR-PM_{2.5} (Organic, sulphate, nitrate, ammonium and
174 chloride), together with meteorological parameters and gas-phase pollutants (SO₂, CO, NO₂
175 and O₃). The average mass concentration of NR-PM_{2.5} was 21.5±14.9 µg m⁻³, similar to the
176 previous AMS/ACSM results in the western China (24.5 µg m⁻³, Xu et al., 2014) and the
177 southeastern China during summer (14.5-32.9 µg m⁻³, Huang et al., 2012; Lee et al., 2013;
178 Huang et al., 2013) but was lower than that in the northern China (41-80 µg m⁻³, Hu et al.,
179 2013; Duan et al., 2020). Organics constituted the largest fraction of NR-PM_{2.5} (35% or 7.5 µg
180 m⁻³), followed by sulphate (25% or 5.3 µg m⁻³), nitrate (17.0% or 3.7 µg m⁻³), ammonium (14%
181 or 3.0 µg m⁻³), BC (8% or 1.7 µg m⁻³), and chloride (1%, 0.2 µg m⁻³).

182 Figure 2 shows the results of winds field map, cluster-averaged backward trajectory and winds
183 rose analyses. Four transport sectors were identified, including the Beijing-Tianjin-Hebei
184 region (BTH, the east cluster, red), the northern China (the north cluster, magenta), the rural
185 Guanzhong Basin region (GZB, the south cluster, green) and the urban GZB region (the west
186 cluster, blue).

187 The BTH transport was featured by the long-distance air mass trajectories advected over the
188 North China Plain with an average wind speed of 1.9±1.8 m s⁻¹. The BTH transport sector
189 accounted for 7% of the total observation days. It showed the highest mass concentration of
190 PM_{2.5} (32.9±17.4 µg m⁻³).

191 The northern China transport sector was clustered by the transport from the Mongolia and the
192 northern part of China, including Inner Mongolia and northern Shaanxi province. It represented
193 the longest transport distance with an average wind speed of 2.2±2.1 m s⁻¹ and accounted for
194 22% of observation days. The PM_{2.5} mass in the northern China transport sector was 24.9±12.9
195 µg m⁻³, which was lower than that in the BTH transport sector.

196 The urban GZB transport sector was from the west of the GZB region, including those large
197 cities in the GZB region, such as Baoji, Xianyang and Xi'an. The urban GZB transport sector
198 was the most frequent pathway during the campaign, accounting for 60% of observation days
199 with an average wind speed of $1.0 \pm 0.9 \text{ m s}^{-1}$. The $\text{PM}_{2.5}$ mass in the urban GZB transport sector
200 was $21.7 \pm 14.8 \mu\text{g m}^{-3}$. Finally, the rural GZB transport sector mainly consisted of the air mass
201 from Mt. Qinling, representing the air mass with least anthropogenic influence and accounting
202 for 11% of observation days with an average wind speed of $1.9 \pm 0.7 \text{ m s}^{-1}$ and the lowest average
203 $\text{PM}_{2.5}$ mass ($8.8 \pm 5.5 \mu\text{g m}^{-3}$).

204 3.2 Secondary inorganic formation during the transport

205 Figure 3 shows the mass concentrations of the measured components, their fractional
206 contributions, the sulphur oxidation ratio (SOR) and the nitrogen oxidation ratio (NOR) in these
207 four transport sectors. SIA showed the highest mass concentration of $21.4 \pm 11.9 \mu\text{g m}^{-3}$ in the
208 BTH transport sector, followed by the northern China transport sector ($15.2 \pm 6.6 \mu\text{g m}^{-3}$), the
209 urban GZB transport sector ($12.2 \pm 3.1 \mu\text{g m}^{-3}$) and the rural GZB transport sector ($3.5 \pm 1.7 \mu\text{g}$
210 m^{-3}). The corresponding fractional contributions of SIA to $\text{PM}_{2.5}$ were 64%, 60%, 55%, and
211 39%. The difference in SIA mass and fractional contributions suggests the difference in SIA
212 precursor concentrations (i.e., SO_2 , NO_x and NH_3) and SIA formation efficiency among
213 different transport sectors, as discussed below.

214 Sulphate was the dominant fraction in the BTH transport sector, accounting for 30% of $\text{PM}_{2.5}$.
215 This fraction decreased to 25% and 24% in the northern China transport sector and the urban
216 GZB transport sector, respectively. Nitrate showed no obvious difference in the three urban
217 transport sectors, accounting for 17-19% of $\text{PM}_{2.5}$. For the rural GZB transport sector, the
218 fraction of sulphate and nitrate largely decreased to 19% and 11% of $\text{PM}_{2.5}$ respectively,
219 consistent with lower SO_2 ($3.2 \pm 2.5 \mu\text{g m}^{-3}$) and NO_2 ($27.8 \pm 10.3 \mu\text{g m}^{-3}$) in the rural GZB
220 transport sector which was about half of that in the three urban transport sectors ($6.3\text{-}7.3 \mu\text{g m}^{-3}$
221 3 for SO_2 and $44.7\text{-}51.3 \mu\text{g m}^{-3}$ for NO_2). High fraction of sulphate in the BTH transport sector
222 was supported by high concentrations of SO_2 and sulphate in the BTH region and central China
223 region (Du et al., 2019; Chen et al., 2020; Li et al., 2021; Sun et al., 2022). It was further
224 supported by high sulphur conversion efficiency (SOR), for which the BTH transport sector
225 showed the highest SOR of 0.58, followed by the northern China transport sector (0.52), the
226 urban GZB transport sector (0.49), and the rural GZB transport sector (0.44) (Figure 3c).
227 Similarly, NOR showed relatively high ~~value-value~~ of 0.29 in the BTH transport sector and the
228 northern China transport sector, and was slightly low in the urban GZB transport sector (0.25)
229 and the rural GZB transport sector (0.24), consistent with high nitrate fraction in the BTH
230 transport sector and the northern China sector (Figure 3d). In comparison with the previously
231 reported results which were investigated in the source regions of the urban GZB transport sector
232 and the BTH transport sector (Xu et al., 2019; Duan et al., 2020, 2021), SOR and NOR showed
233 obvious increase after transport. For SOR it increased from 0.36 to 0.44 in the urban GZB
234 transport pathway and from 0.53 to 0.58 in the BTH transport pathway, while for NOR it
235 increased from 0.06 to 0.25 in the urban GZB transport pathway and from 0.15 to 0.29 in the
236 BTH transport pathway. The increases in SOR and NOR after transport suggest the efficient
237 sulphate and nitrate formation during the regional transport. This was also reflected in the

238 sulphate and nitrate fractions (Figure 4). After transport the fractional contribution of sulphate
239 increased from 17% ($3.8 \mu\text{g m}^{-3}$) to 26% ($5.6 \mu\text{g m}^{-3}$) in the urban GZB transport pathway and
240 from 20% ($6.2 \mu\text{g m}^{-3}$) to 32% ($9.9 \mu\text{g m}^{-3}$) in the BTH transport pathway, while the nitrate
241 fraction increased from 12% ($2.7 \mu\text{g m}^{-3}$) to 19% ($3.7 \mu\text{g m}^{-3}$) in the urban GZB transport
242 pathway but slightly decreased from 24% ($7.4 \mu\text{g m}^{-3}$) to 19% ($5.9 \mu\text{g m}^{-3}$) in the BTH transport
243 pathway likely due to ~~the volatilization of NH_4NO_3 during the long-distance transport. the mass~~
244 ~~loss of semi-volatile aerosol species (such as NH_4NO_3) when aerosols are exposed to a cleaner~~
245 ~~environment during the long-distance transport (Liu et al., 2021).~~ We also compared the
246 pollution episodes caused by the continuous transport from the BTH (EP1) and the urban GZB
247 (EP2) (as shown in the shaded area in Figure 1, detailed in Fig. S3). Sulphate and nitrate were
248 normalized by BC to minimize the influence of primary emission or dilution (Figure 5).
249 Sulphate/BC ratio increased with the transport in both EP1 and EP2, with a growth rate of 0.26
250 hr^{-1} during EP1 (increased from 1.2 to 9.4 in 31 hours) and of 0.1 hr^{-1} during EP2 (increased
251 from 2.3 to 16.2 in 131 hours). Nitrate/BC ratio showed a growth rate of 0.17 hr^{-1} during EP1
252 (increased from 1.3 to 6.6 in 31 hours) and of 5.7 times lower during EP2 (0.03 hr^{-1} , increased
253 from 1.1 to 4.7 in 131 hours). The comparison of these two episodes further supports stronger
254 formation of SIA in the BTH transport sector. The difference in the formation efficiency of
255 sulphate and nitrate in different transport air masses may be related to RH, because aqueous-
256 phase oxidation was an important formation pathway for sulphate at high RH condition (Cheng
257 et al., 2016; Xue et al., 2019; Chang et al., 2020) and high RH also strengthened the conversion
258 of gas-phase NH_4NO_3 to particle phase (Huang et al., 2020), which likely leads to high SOR
259 and NOR in the BTH transport sector ($81 \pm 17\%$ of average RH).

260 3.3 Secondary organic formation during the transport

261 Figure 6 shows the mass concentrations of the resolved OA factors, their fractional
262 contributions, the f_{44} versus f_{43} ratio and O/C ratio in these four transport sectors. f_{44}/f_{43} ratio
263 and O/C ratio are important indicators of the oxidation state of bulk OA (Ng et al., 2010), which
264 were widely used in previous studies for SOA oxidation analysis (Xu et al., 2014; Canonaco et
265 al., 2015; Reyes-Villegas et al., 2016). The BTH transport sector showed the highest OA mass
266 concentration of $8.9 \pm 5.1 \mu\text{g m}^{-3}$, followed by the urban GZB transport sector ($7.3 \pm 4.0 \mu\text{g m}^{-3}$),
267 the northern China transport sector ($6.9 \pm 3.9 \mu\text{g m}^{-3}$) and the rural GZB transport sector ($4.6 \pm$
268 $2.5 \mu\text{g m}^{-3}$). The corresponding fractional contributions of MO-OOA to total OA were 58% (5.2
269 $\mu\text{g m}^{-3}$), 55% ($4.0 \mu\text{g m}^{-3}$), 57% ($4.0 \mu\text{g m}^{-3}$), and 42% ($1.9 \mu\text{g m}^{-3}$), constituting the major OA
270 source in the four transport sectors. The LO-OOA fraction was higher in the rural GZB transport
271 sector (34%, $1.9 \mu\text{g m}^{-3}$) compared to the other three urban transport sectors (around 23%, 3.9 -
272 $5.2 \mu\text{g m}^{-3}$), suggesting that SOA was less oxidized in the rural transport sector ~~likely due to~~
273 ~~large emission of biogenic VOCs from the Mt. Qinling area.~~ The northern China transport sector
274 showed the highest f_{44}/f_{43} ratio of 2.1 and O/C ratio of 0.87, followed by the BTH transport
275 sector (1.9 and 0.78), the urban GZB transport sector (1.8 and 0.72), and much lower values in
276 the rural GZB transport sector (1.6 and 0.58). The higher f_{44}/f_{43} and O/C ratio in the northern
277 China transport sector and the BTH transport sector suggests sufficient OA aging during long-
278 range transport. The f_{44}/f_{43} ratios in these four transport sectors were higher than those in the
279 urban sites in previous studies (triangle in Figure 6c, Ng et al., 2011) and the O/C ratios in these

280 four transport sectors (0.72-0.87) were also much higher than those measured in urban sites in
281 China during summer, such as Lanzhou (0.33, Xu et al., 2014) and Jiaxing (0.28, Huang et al.,
282 2013), but similar to the results from the mountainous site in North China Plain during summer
283 (0.75, Li et al., 2021) and the long-range transport study in the United States (0.8, Gunsch et
284 al., 2018). ~~but similar to the result from the long-range transport study in the United States (0.8,~~
285 ~~Gunseh et al., 2018).~~ Note that the O/C ratios in the transport sectors were also much higher
286 than those measured in the source regions of the urban GZB transport sector and the BTH
287 transport sector, with O/C ratio increasing from 0.54 to 0.78 in the BTH transport pathway and
288 from 0.58 to 0.72 in the urban GZB transport pathway after transport. The corresponding MO-
289 OOA to SOA fraction also increased from 37% ($3.4 \mu\text{g m}^{-3}$) to 72% ($5.2 \mu\text{g m}^{-3}$) in the BTH
290 transport pathway and from 37% ($3.6 \mu\text{g m}^{-3}$) to 70% ($4.0 \mu\text{g m}^{-3}$) in the urban GZB transport
291 pathway (Figure 7), suggesting regional transport enhanced OA aging process and thus the OA
292 oxidation state. The growth rates of MO-OOA and LO-OOA during the pollution episodes of
293 EP1 and EP2 are shown in Figure 8. Similar to SIA, MO-OOA/BC ratio increased with the
294 transport duration for both episodes. It showed a growth rate of 0.15 hr^{-1} during EP1 (increased
295 from 0.23 to 4.77 in 31 hours) and of 0.06 hr^{-1} during EP2 (increased from 1.58 to 9.59 in 131
296 hours), suggesting stronger formation of MO-OOA in the BTH transport sector. On the contrary,
297 LO-OOA showed no obvious increasing trend with the transport duration during EP1 and EP2,
298 likely due to a higher conversion efficiency from LO-OOA to MO-OOA.

299 **4. Conclusion**

300 The observation at ~200 m above the ground in the junction of North China Plain and Fenwei
301 Basin showed that the fraction of SIA and MO-OOA increased significantly after transport. The
302 sulfur oxidation rate (SOR, 0.49-0.58), nitrogen oxidation rate (NOR, 0.25-0.29), f_{44}/f_{43} ratio
303 (1.6-2.1) and O/C ratio (0.72-0.87) were significantly higher than those investigated locally,
304 indicating that long-distance transport largely enhanced the SIA formation, the OA oxidation
305 and aging. The formation rate of sulphate, nitrate and MO-OOA in the BTH transport sector
306 was much higher than that in the GZB transport sector, indicating the stronger sulphate, nitrate
307 and MO-OOA formation efficiency in the BTH transport sector.

308 **5. Data availability**

309 The detailed data can be obtained from <https://doi.org/10.5281/zenodo.6446514> (Zhong et al.,
310 2022).

311 **Acknowledgement**

312 This work was supported by the National Natural Science Foundation of China (NSFC) under
313 Grant No. 41925015 and 41877408, the Chinese Academy of Sciences (no. ZDBS-LY-
314 DQC001), and the Cross Innovative Team fund from the State Key Laboratory of Loess and
315 Quaternary Geology (No. SKLLQGTD1801).

316 **Author contributions**

317 **Haobin Zhong:** Methodology, data curation, Formal analysis, Writing – original draft, Writing

318 – review & editing. **Ru-jin Huang**: Conceptualization, Validation, Data curation, Writing –
319 original draft, Writing – review & editing, Supervision, Project administration, Funding
320 acquisition. **Chunshui Lin**: Writing - review & editing. **Wei Xu**: Writing - review & editing.
321 **Jing Duan**: Writing - review & editing. **Yifang Gu**: Writing - review & editing. **Wei Huang**:
322 Writing - review & editing. **Haiyan Ni**: Writing - review & editing. **Chongshu Zhu**: Resources.
323 **Yan You**: Writing - review & editing. **Yunfei Wu**: Resources. **Renjian Zhang**: Resources.
324 **Jurgita Ovadnevaite**: Writing - review & editing. **Darius Ceburnis**: Writing - review &
325 editing. **Colin D. O'Dowd**: Writing - review & editing.

326 **Competing interests**

327 The authors have no competing interests to declare.

328 **Reference**

329 An, Z., Huang, R., Zhang, R., Tie, X., Li, G., Cao, J., Zhou, W., Shi, Z., Han, Y., Gu, Z., Ji, Y.:
330 Severe haze in northern China: A synergy of anthropogenic emissions and atmospheric
331 processes. *Proc. Natl. Acad. Sci.* 116, 8657–8666, 2019.

332 Braun, R., Aghdam, M., Bañaga, P., Betito, G., Cambaliza, M., Cruz, M., Lorenzo,
333 G., MacDonald, A., Simpas, J., Stahl, C., Sorooshian, A.: Long-range aerosol transport and
334 impacts on size-resolved aerosol composition in Metro Manila, Philippines. *Atmos. Chem.*
335 *Phys.*, 20, 2387–2405, 2020.

336 Canagaratna, M., Jayne, J., Jimenez, J., Allan, J., Alfarra, M., Zhang, Q., Onasch, T., Drewnick,
337 F., Coe, H., Middlebrook, A., Delia, A., Williams, L., Trimborn, A., Northway, M., DeCarlo,
338 P., Kolb, C., Davidovits, P., and Worsnop, D.: Chemical and microphysical characterization
339 of ambient aerosols with the Aerodyne aerosol mass spectrometer, *Mass Spectrom. Rev.*
340 26(2), 185–222, 2007.

341 Canonaco, F., Crippa, M., Slowik, J., Baltensperger, U., and Prévôt, A.: SoFi, an Igor based
342 interface for the efficient use of the generalized multilinear engine (ME-2) for source
343 apportionment: application to aerosol mass spectrometer data. *Atmos. Meas. Tech.* 6(12),
344 3649-3661, 2013.

345 Canonaco, F., Slowik, J. G., Baltensperger, U., and Prévôt, A. S. H.: Seasonal differences in
346 oxygenated organic aerosol composition: implications for emissions sources and factor
347 analysis, *Atmos. Chem. Phys.*, 15, 6993–7002, 2015.

348 Cao, J., Wang, Q., Chow, J., Watson, J., Tie, X., Shen, Z., Wang, P., An, Z.: Impacts of aerosol
349 compositions on visibility impairment in Xi'an, China. *Atmos. Environ.* 59, 559-566, 2012.

350 Calvo, A., Alves, C., Castro, A., Pont, V., Vicente, A., and Fraile, R.: Research on aerosol
351 sources and chemical composition: past, current and emerging issues, *Atmos. Res.*, 120, 1–
352 28, 2013.

353 Chang, Y., Huang, R.-J., Ge, X., Huang, X., Hu, J., Duan, Y., Zou, Z., Liu, X., and Lehmann.

354 M.F.: Puzzling haze events in China during the coronavirus (COVID-19) shutdown.
355 GEOPHYS. RES. LETT. 47(12), e2020GL088533, 2020.

356 Chen, T., Liu, J., Liu, Y., Ma, Q., Ge, Y., Zhong, C., Jiang, H., Chu, B., Zhang, P., Ma, J., Liu,
357 P., Wang, Y., Mu, Y., He, H.: Chemical characterization of submicron aerosol in summertime
358 Beijing: A case study in southern suburbs in 2018. *Chemosphere*. 247, 125918, 2020.

359 Chen, W., Ye, Y., Hu, W., Zhou, H., Pan, T., Wang, Y., Song, W., Song, Q., Ye, C., Wang, C.,
360 Wang, B., Huang, S., Yuan, B., Zhu, M., Lian, X., Zhang, G., Bi, X., Jiang, F., Liu, J.,
361 Canonaco, F., Prévôt, A., Shao, M., Wang, X.: Real-time characterization of aerosol
362 compositions, sources, and aging processes in Guangzhou during PRIDE-GBA 2018
363 campaign. *Journal of Geophysical Research: Atmospheres*, 126, e2021JD035114, 2021.

364 Cheng, Y., Zheng, G., Wei, C., Mu, Q., Zheng, B., Wang, Z., Gao, M., Zhang, Q., He, K.,
365 Carmichael, G., Poschl, U., Su, H.: Reactive nitrogen chemistry in aerosol water as a source
366 of sulfate during haze events in China. *Sci. Adv.*, 2(12), e1601530, 2016.

367 Cohen, A., Brauer, M., Burnett, R., Anderson, H., Frostad, J., Estep, K., Balakrishnan, K.,
368 Brunekreef, B., Dandona, L., Dandona, R., Feigin, V., Freedman, G., Hubbell, B., Jobling,
369 A., Kan, H., Knibbs, L., Liu, Y., Martin, R., Morawska, L., Pope III, C., Shin, H., Straif, K.,
370 Shaddick, G., Thomas, M., van Dingenen, R., van Donkelaar, A., Vos, T., Murray, C., and
371 Forouzanfar, M.: Estimates and 25-year trends of the global burden of disease attributable to
372 ambient air pollution: an analysis of data from the Global Burden of Diseases Study 2015.
373 *The Lancet*, 389(10082), 1907–1918, 2017.

374 Das, S. and Jayaraman, A.: Long-range transportation of anthropogenic aerosols over eastern
375 coastal region of India: investigation of sources and impact on regional climate change.
376 *Atmos. Res.*, 118, 68-83, 2012.

377 DeCarlo, P., Ulbrich, I., Crouse, J., de Foy, B., Dunlea, E., Aiken, A., Knapp, D., Weinheimer,
378 A., Campos, T., Wennberg, P., Jimenez, J.: Investigation of the sources and processing of
379 organic aerosol over the Central Mexican Plateau from aircraft measurements during
380 MILAGRO. *Atmos. Chem. Phys.* 10(12), 5257–5280, 2010.

381 Draxler, R.R. and Hess, G.D.: An overview of the HYSPLIT_4 modelling system for
382 trajectories, dispersion, and deposition. *Australian Meteorological Magazine*, 47, 295-308,
383 1998.

384 Duan, J., Huang, R.-J., Lin, C., Dai, W., Wang, M., Gu, Y., Wang, Y., Zhong, H., Zheng, Y., Ni,
385 H., Dusek, U., Chen, Y., Li, Y., Chen, Q., Worsnop, D.R., O'Dowd, C.D., Cao, J.J.:
386 Distinctions in source regions and formation mechanisms of secondary aerosol in Beijing
387 from summer to winter. *Atmos. Chem. Phys.* 19, 10319–10334, 2019.

388 Duan, J., Huang, R., Li, Y., Chen, Q., Zheng, Y., Chen, Y., Lin, C., Ni, H., Wang, M.,
389 Ovadnevaite, J., Ceburnis, D., Chen, C., Worsnop, D.R., Hoffmann, T., O'Dowd, C., Cao,
390 J.J.: Summertime and wintertime atmospheric processes of secondary aerosol in Beijing.
391 *Atmos. Chem. Phys.* 20, 3793–3807, 2020.

392 Duan, J., Huang, R.-J., Gu, Y., Lin, C., Zhong, H., Wang, Y., Yuan W., Ni, H., Yang, L., Chen,
393 Y., Worsnop, D., O'Dowd, C.: The formation and evolution of secondary organic aerosol
394 during summer in Xi'an: Aqueous phase processing in fog-rain days. *Sci. Total Environ.* 756
395 (20), 144077, 2021.

396 Du, H., Li, J., Chen, X., Wang, Z., Sun, Y., Fu, P., Li, J., Gao, J., and Wei, Y.: Modeling of
397 aerosol property evolution during winter haze episodes over a megacity cluster in northern
398 China: roles of regional transport and heterogeneous reactions of SO₂, *Atmos. Chem. Phys.*,
399 19, 9351–9370, 2019.

400 Elser, M., Huang, R., Wolf, R., Slowik, J., Wang, Q., Canonaco, F., Li, G., Bozzetti, C.,
401 Daellenbach, K., Huang, Y., Zhang, R., Li, Z., Cao, J., Baltensperger, U., El-Haddad, I.,
402 Prévôt, A.: New insights into PM_{2.5} chemical composition and sources in two major cities in
403 China during extreme haze events using aerosol mass spectrometry. *Atmos. Chem. Phys.* 16,
404 3207–3225, 2016.

405 Feng, T., Bei, N., Zhao, S., Wu, J., Li, X., Zhang, T., Cao, J., Zhou, W., Li, G.: Wintertime
406 nitrate formation during haze days in the Guanzhong basin, China: a case study. *Environ.*
407 *Pollut.*, 243, 1057-1067, 2018.

408 Fierce, L., Bond, T. C., Bauer, S. E., Mena, F., and Riemer, N.: Black carbon absorption at the
409 global scale is affected by particle-scale diversity in composition, *Nat. Commun.*, 7, 12361,
410 2016.

411 Fröhlich, R., Cubison, M., Slowik, J., Bukowiecki, N., Prévôt, A., Baltensperger, U., Schneider,
412 J., Kimmel, J., Gonin, M., Rohner, U., Worsnop, D., Jayne, J.: The ToF-ACSM: a portable
413 aerosol chemical speciation monitor with TOFMS detection, *Atmos. Meas. Tech.*, 6(11),
414 3225-3241, 2013.

415 Gunsch, M. J., May, N. W., Wen, M., Bottenus, C. L. H., Gardner, D. J., VanReken, T. M.,
416 Bertman, S. B., Hopke, P. K., Ault, A. P., and Pratt, K. A.: Ubiquitous influence of wildfire
417 emissions and secondary organic aerosol on summertime atmospheric aerosol in the forested
418 Great Lakes region, *Atmos. Chem. Phys.*, 18, 3701–3715, 2018.

419 Guo, J., Zhou, S., Cai, M., Zhao, J., Song, W., Zhao, W., Hu, W., Sun, Y., He, Y., Yang, C., Xu,
420 X., Zhang, Z., Cheng, P., Fan, Q., Hang, J., Fan, S., Wang, X., and Wang, X.: Characterization
421 of submicron particles by time-of-flight aerosol chemical speciation monitor (ToF-ACSM)
422 during wintertime: aerosol composition, sources, and chemical processes in Guangzhou,
423 China, *Atmos. Chem. Phys.*, 20, 7595–7615, 2020.

424 Hao, J., Lv, Z., Chu, B., Wu, S., Zhao, Z., et al.: Characterization, Experimental study, and
425 Modeling of Atmospheric Secondary Organic Aerosol [M]. Beijing: Science Press., 83-94,
426 2015.

427 Huang, Y., Li, L., Li, J., Wang, X., Chen, H., Chen, J., Yang, X., Gross, D., Wang, H., Qiao, L.,
428 Chen, C.: A case study of the highly time-resolved evolution of aerosol chemical and optical
429 properties in urban Shanghai, China. *Atmos. Chem. Phys.* 13, 3931–3944, 2013.

430 Huang, R., Zhang, Y., Bozzetti, C., Ho, K., Cao, J., Han, Y., Daellenbach, K.R., Slowik, J.G.,
431 Platt, S.M., Canonaco, F.: High secondary aerosol contribution to particulate pollution during
432 haze events in China. *Nature* 514 (7521), 218-222, 2014.

433 Huang, R.-J., Wang, Y., Cao, J., Lin, C., Duan, J., Chen, Q., Li, Y., Gu, Y., Yan, J., Xu, W.,
434 Fröhlich, R., Canonaco, F., Bozzetti, C., Ovadnevaite, J., Ceburnis, D., Canagaratna, M.R.,
435 Jayne, J., Worsnop, D.R., El-Haddad, I., Prévôt, A.S.H., O’Dowd, C.D.: Primary emissions
436 versus secondary formation of fine particulate matter in the most polluted city (Shijiazhuang)
437 in North China. *Atmos. Chem. Phys.* 19, 2283–2298, 2019.

438 Huang, X., He, L., Xue, L., Sun, T., Zeng, L., Gong, Z. H., Hu, M., and Zhu, T.: Highly time-
439 resolved chemical characterization of atmospheric fine particles during 2010 shanghai world
440 expo, *Atmos. Chem. Phys.*, 12, 4897–4907, 2012.

441 Huang, X., Xue, L., Tian, X., Shao, W., Sun, T., Gong, Z., Ju, W., Jiang, B., Hu, M., and He, L.:
442 Highly time-resolved carbonaceous aerosol characterization in yangtze river delta of china:
443 Composition, mixing state and secondary formation, *Atmos. Environ.*, 64, 200–207, 2013.

444 Huang, X., Ding, A., Wang, Z., Ding, K., Gao, J., Chai, F., Fu, C.: Amplified transboundary
445 transport of haze by aerosol–boundary layer interaction in China. *Nature Geosci.*, 13, 428-
446 434, 2020.

447 Hu, W., Hu, M., Yuan, B., Jimenez, J., Tang, Q., Peng, J., Hu, W., Shao, M., Wang, M., Zeng,
448 L., Wu, Y., Gong, Z., Huang, X., and He, L.: Insights on organic aerosol aging and the
449 influence of coal combustion at a regional receptor site of central eastern china, *Atmos.*
450 *Chem. Phys.*, 13, 10095–10112, 2013.

451 Ji, Y., Qin, X., Wang, B., Xu, J., Shen, J., Chen, J., Huang, K., Deng, C., Yan, R., Xu, K., and
452 Zhang, T.: Counteractive effects of regional transport and emission control on the formation
453 of fine particles: a case study during the Hangzhou G20 summit, *Atmos. Chem. Phys.*, 18,
454 13581–13600, 2018.

455 Kim, H., Zhang, Q., and Heo, J.: Influence of intense secondary aerosol formation and long-
456 range transport on aerosol chemistry and properties in the Seoul Metropolitan Area during
457 spring time: results from KORUS-AQ, *Atmos. Chem. Phys.*, 18, 7149–7168, 2018.

458 Kindap, T., Unal, A., Chen, S., Hu, Y., Odman, M., Karaca, M.: Long-range aerosol transport
459 from Europe to Istanbul, Turkey. *Atmos, Environ.*, 40(19), 3536-3547, 2006.

460 Lee, B; Li, Y; Yu, J.; Louie, P; Chan, C.: Physical and chemical characterization of ambient
461 aerosol by HR-ToF-AMS at a suburban site in Hong Kong during springtime 2011. *J.*
462 *GEOPHYS. RES.*, 118(15), 8625–8639, 2013.

463 Lei, Y., Zhang, Q., He, K., Streets, D.: Primary anthropogenic aerosol emission trends for China,
464 1990–2005. *Atmos. Chem. Phys.* 11, 931–954, 2011.

465 Lelieveld, J., Evans, J. S., Fnais, M., Giannadaki, D., and Pozzer, A.: The contribution of
466 outdoor air pollution sources to premature mortality on a global scale, *Nature*, 525, 367–371,
467 2015.

- 468 Li, Y., Lee, B., Su, L., Fung, J., Chan, C.: Seasonal characteristics of fine Journal Pre-proof
469 Journal Pre-proof 23 particulate matter (PM) based on high -resolution time -of-flight aerosol
470 mass spectrometric (HR -ToF -AMS) measurements at the HKUST Supersite in Hong Kong.
471 Atmos. Chem. Phys. 15(1), 37 -53, 2015.
- 472 Li, H., Cheng, J., Zhang, Q., Zheng, B., Zhang, Y., Zheng, G., He, K.: Rapid transition in winter
473 aerosol composition in Beijing from 2014 to 2017: response to clean air actions. Atmos.
474 Chem. Phys. 19, 11485–11499, 2019.
- 475 Li, J. and Han, Z.: A modeling study of severe winter haze events in Beijing and its neighboring
476 regions, Atmos. Res., 170, 87–97, 2016.
- 477 Li, J., Du, H., Wang, Z., Sun, Y., Yang, W., Li, J., Tang, X., and Fu, P.: Rapid formation of a
478 severe regional winter haze episode over a mega-city cluster on the North China Plain,
479 Environ. Pollut., 223, 605–615, 2017.
- 480 Li, J., Liu, Z., Cao, L., Gao, W., Yan, Y., Mao, J., Zhang, X., He, L., Xin, J., Tang, G., Ji, D.,
481 Hu, B., Wang, L., Wang, Y., Dai, L., Zhao, D., Du, W., Wang, Y.: Highly time-resolved
482 chemical characterization and implications of regional transport for submicron aerosols in
483 the North China Plain, Sci. Total. Environ., 705, 135803, 2021.
- 484 [Li, J., Cao, L., Gao, W., He, L., Yan, Y., He, Y., Pan, Y., Ji, D., Liu, Z., and Wang, Y.: Seasonal](#)
485 [variations in the highly time-resolved aerosol composition, sources and chemical processes](#)
486 [of background submicron particles in the North China Plain, Atmos. Chem. Phys., 21, 4521–](#)
487 [4539, 2021.](#)
- 488 Lin, C., Huang, R.-J., Duan, J., Zhong, H., Xu, W., Wu, Y., Zhang, R.: Large contribution from
489 worship activities to the atmospheric soot particles in northwest China. Environ. Pollut.
490 299(15), 118907, 2022.
- 491 Liu, P., Zhang, Y., Wu, T., Shen, Z., Xu, H.: Acid -extractable heavy metals in PM_{2.5} over Xi'an,
492 China: seasonal distribution and meteorological influence. Environ Sci Pollut Res. 26 (33),
493 34357 -34367, 2019.
- 494 [Liu, Q., Liu, D., Wu, Y., Bi, K., Gao, W., Tian, P., Zhao, D., Li, S., Yu, C., Tang, G., Wu, Y., Hu,](#)
495 [K., Ding, S., Gao, Q., Wang, F., Kong, S., He, H., Huang, M., and Ding, D.: Reduced](#)
496 [volatility of aerosols from surface emissions to the top of the planetary boundary layer,](#)
497 [Atmos. Chem. Phys., 21, 14749–14760, 2021.](#)
- 498 [Liu, Z., Gao, W., Yu, Y., Hu, B., Xin, J., Sun, Y., Wang, L., Wang, G., Bi, X., Zhang, G., Xu, H.,](#)
499 [Cong, Z., He, J., Xu, J., and Wang, Y.: Characteristics of PM_{2.5} mass concentrations and](#)
500 [chemical species in urban and background areas of China: emerging results from the CARE-](#)
501 [China network, Atmos. Chem. Phys., 18, 8849–8871, 2018.](#)
- 502 Middlebrook, A., Bahreini, R., Jimenez, J., Canagaratna, M.: Evaluation of composition-
503 dependent collection efficiencies for the aerodyne aerosol mass spectrometer using field data.
504 Aerosol Sci. Tech. 46(3), 258-271, 2012.
- 505 Moffet, R. C. and Prather, K. A.: In-situ measurements of the mixing state and optical properties

506 of soot with implications for radiative forcing estimates. *P. Natl. Acad. Sci.*, 106, 11872–
507 11877, 2009.

508 Ng, N., Canagaratna, M., Zhang, Q., Jimenez, J., Tian, J., Ulbrich, I., Kroll, J., Docherty, K.,
509 Chhabra, P., Bahreini, R., Murphy, S., Seinfeld, J., Hildebrandt, L., Donahue, N., DeCarlo,
510 P., Lanz, V., Prévôt, A., Dinar, E., Rudich, Y. and Worsnop, D.: Organic aerosol components
511 observed in Northern Hemispheric datasets from Aerosol Mass Spectrometry. *Atmos. Chem.*
512 *Phys.*, 10, 4625–4641, 2010.

513 Paatero, P. and Tapper, U.: Positive Matrix Factorization: a nonnegative factor model with
514 optimal utilization of error estimates of data values. *Environmetrics*. 5(2), 111-126, 1994.

515 Paatero, P.: Least squares formulation of robust non-negative factor analysis. *Chemom. Intell.*
516 *Lab.* 37(1), 23-35, 1997.

517 Paatero, P.: The multilinear engine: a table-driven, least squares program for solving multilinear
518 problems, including the n-way parallel factor analysis model. *J. Comput. Graph. Stat.* 8(4),
519 854-888, 1999.

520 Pandis, N., Harley, R., Cass, G., Seinfeld, J.: Secondary organic aerosol formation and transport.
521 *Atmos. Environ.*, 26(13), 2269-2282, 1992.

522 Pu, W., Zhao, X., Shi, X., Ma, Z., Zhang, X., Bo, Y.: Impact of long-range transport on aerosol
523 properties at a regional background station in Northern China. *Atmos. Res.*, 153, 489-499,
524 2015.

525 Reyes-Villegas, E., Green, D. C., Priestman, M., Canonaco, F., Coe, H., Prévôt, A. S. H., and
526 Allan, J. D.: Organic aerosol source apportionment in London 2013 with ME-2: exploring
527 the solution space with annual and seasonal analysis, *Atmos. Chem. Phys.*, 16, 15545–15559,
528 2016.

529 Riemer, N. and West, M.: Quantifying aerosol mixing state with entropy and diversity measures,
530 *Atmos. Chem. Phys.*, 13, 11423–11439, 2013.

531 Salvador, P., Artinano, B., Querol, X., Alastuey, A.: A combined analysis of backward
532 trajectories and aerosol chemistry to characterize long-range transport episodes of particulate
533 matter. The Madrid air basin, a case study. *Sci. Total Environ.*, 390, 495-506, 2008.

534 Schichtel, B., Gebhart, K., Barna, M., Malm, W.: Association of air mass transport patterns and
535 particulate sulfur concentrations at Big Bend National Park, Texas. *Atmos. Environ.*, 40, 992-
536 1006, 2006.

537 Shen, Z., Cao, J., Liu, S., Zhu, C., Wang, X., Zhang, T., Xu, H., Hu, T.: Chemical composition
538 of PM10 and PM2.5 collected at ground level and 100 meters during a strong winter-time
539 pollution episode in Xi'an, China. *J. AIR WASTE MANAGE.*, 61, 1150–1159, 2011.

540 Srivastava, D., Favez, O., Perraudin, E., Villenave, E., & Albinet, A.: Comparison of
541 measurement-based methodologies to apportion secondary organic carbon (SOC) in PM2.5:
542 a review of recent studies. *Atmosphere*, 9(11), 452, 2018.

- 543 Sun, Y., Wang, Z., Fu, P., Yang, T., Jiang, Q., Dong, H., Li, J., Jia, J.: Aerosol composition,
544 sources and processes during wintertime in Beijing, China. *Atmos. Chem. Phys.* 13, 4577–
545 4592, 2013.
- 546 Sun, C., Lee, B., Huang, D., Jie Li, Y., Schurman, M., Louie, P., Luk, C., Chan, C.: Continuous
547 measurements at the urban roadside in an Asian megacity by Aerosol Chemical Speciation
548 Monitor (ACSM): particulate matter characteristics during fall and winter seasons in Hong
549 Kong. *Atmos. Chem. Phys.* 16(3), 1713 -1728, 2016.
- 550 [Sun, P., Nie, W., Chi, X., Huang, X., Ren, C., Xue, L., Shan, Y., Wen L., Li, H., Chen, T., Qi,](#)
551 [Y., Gao, J., Zhang, Q., and Ding, A.: Aircraft study of secondary aerosols in long-range](#)
552 [transported air masses from the North China Plain by a mid-latitude cyclone. *Journal of*](#)
553 [*Geophysical Research: Atmospheres*, 127, e2021JD036178, 2022.](#)
- 554 Tang, L., Eugenson, M., Sjöberg, K., Wichmann, J.: Estimation of the long-range transport
555 contribution from secondary inorganic components to urban background PM10
556 concentrations in south-western Sweden during 1986–2010. *Atmos. Environ.*, 89, 93-101,
557 2014.
- 558 Tang, G., Zhang, J., Zhu, X., Song, T., Münkel, C., Hu, B., Schäfer, K., Liu, Z., Zhang, J., Wang,
559 L., Xin, J., Suppan, P., and Wang, Y.: Mixing layer height and its implications for air pollution
560 over Beijing, China, *Atmos. Chem. Phys.*, 16, 2459–2475, 2016.
- 561 Tie, X., Huang, R.-J., Dai, W., Cao, J., Long, X., Su, X., Zhao, S., Wang, Q., Li, G.: Effect of
562 heavy haze and aerosol pollution on rice and wheat productions in China. *Sci. Rep.* 6(1),
563 29612, 2016.
- 564 Tie, X. and Cao, J.: Aerosol pollution in China: Present and future impact on environment.
565 *Particuology*. 7(6), 426-431, 2009.
- 566 Updyke, K., Nguyen, T., Nizkorodov, S.: Formation of brown carbon via reactions of ammonia
567 with secondary organic aerosols from biogenic and anthropogenic precursors. *Atmos.*
568 *Environ.*, 63, 22-31, 2012.
- 569 Uno, I., Eguchi, K., Yumimoto, K., Takemura, T., Shimizu, A., Uematsu, M., Liu, Z., Wang, Z.,
570 Hara, Y., and Sugimoto, N.: Asian dust transported one full circuit around the globe, *Nat.*
571 *Geosci.*, 2, 557–560, 2009.
- 572 Wang, Y., Huang, R., Ni, H., Chen, Y., Wang, Q., Li, G., Tie, X., Shen, Z., Huang, Y., Liu, S.,
573 Dong, W., Xue, P., Frohlich, R., Canonaco, F., Elser, M., Daellenbach, K., Bozzetti, C., El-
574 Haddad, I., Prévôt, A., Canagaratna, M., Worsnop, D., Cao, J.: Chemical composition,
575 sources and secondary processes of aerosols in Baoji city of northwest China. *Atmos.*
576 *Environ.* 158, 128 -137, 2017.
- 577 Wang, H., Wang, Q., Gao, Y., Zhou, M., Jing, S., Qiao, L., Yuan, B., Huang, D., Huang, C., Lou,
578 S., Yan, R., Gouw, J., Zhang, X., Chen, J., Chen, C., Tao, S., An, J., Li, Y.: Estimation of
579 Secondary Organic Aerosol Formation During a Photochemical Smog Episode in Shanghai,
580 China. *Journal of Geophysical Research: Atmospheres*. 125(7), e2019JD032033, 2020.

581 Wehner, B., Philippin, S., Wiedensohler, A., Scheer, V., and Vogt, R.: Variability of non-volatile
582 fractions of atmospheric aerosol particles with traffic influence, *Atmospheric Environment*,
583 38, 6081–6090, 2004.

584 Wu, C., & Yu, J. Z.: Determination of primary combustion source organic carbon-toelemental
585 carbon (OC/EC) ratio using ambient OC and EC measurements: secondary OC-EC
586 correlation minimization method. *Atmos. Chem. Phys.*, 16(8), 5453–5465, 2016.

587 Xu, J., Tao, J., Zhang, R., Cheng, T., Leng, C., Chen, J., Huang, G., Li, X., Zhu, Z.:
588 Measurements of surface aerosol optical properties in winter of Shanghai. *Atmos. Res.* 109-
589 110, 25-35, 2012.

590 Xu, J., Zhang, Q., Chen, M., Ge, X., Ren, J., Qin, D.: Chemical composition, sources, and
591 processes of urban aerosols during summertime in northwest China: insights from high-
592 resolution aerosol mass spectrometry. *Atmos. Chem. Phys.*, 14, 12593–12611, 2014.

593 Xu, W., Xie, C., Karnezi, E., Zhang, Q., Wang, J., Pandis, S., Ge, X., Zhang, J., An, J., Wang,
594 Q., Zhao, J., Du, W., Qiu, Y., Zhou, W., He, Y., Li, Y., Li, J., Fu, P., Wang, Z., Worsnop, D.,
595 Sun, Y.: Summertime aerosol volatility measurements in Beijing, China. *Atmos. Chem. Phys.*
596 19, 10205-10216, 2019.

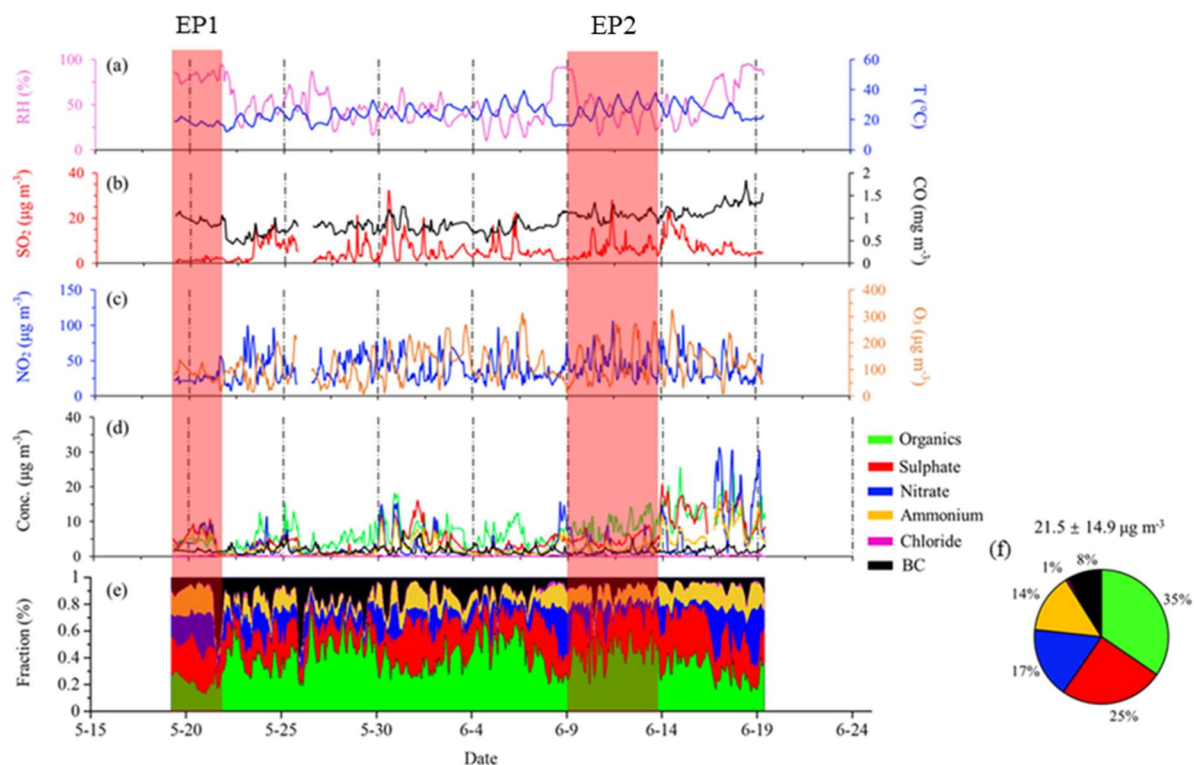
597 Yang, Y. R., Liu, X. G., Qu, Y., Wang, J. L., An, J. L., Zhang, Y., and Zhang, F.: Formation
598 mechanism of continuous extreme haze episodes in the megacity Beijing, China, in January
599 2013, *Atmos. Res.*, 155, 192–203, 2015.

600 Zhang, K., Leeuw, G., Yang, Z., Chen, X., Su, X., Jiao, J.: Concentrations Using VIIRS-Derived
601 AOD in the Guanzhong Basin, China. *Remote Sens.*, 11(22), 2679, 2019.

602 Zhang, Q., Shen, Z., Zhang, L., Zheng, Y., Ning, Z., Zhang, T., Lei, Y., Wang, Q., Li, G., Sun,
603 J., Westerdahl, D., Xu, H., Cao, J.: Investigation of Primary and Secondary Particulate Brown
604 Carbon in Two Chinese Cities of Xi’an and Hong Kong in Wintertime. *Environ. Sci. Technol.*,
605 54, 7, 3803–3813, 2020.

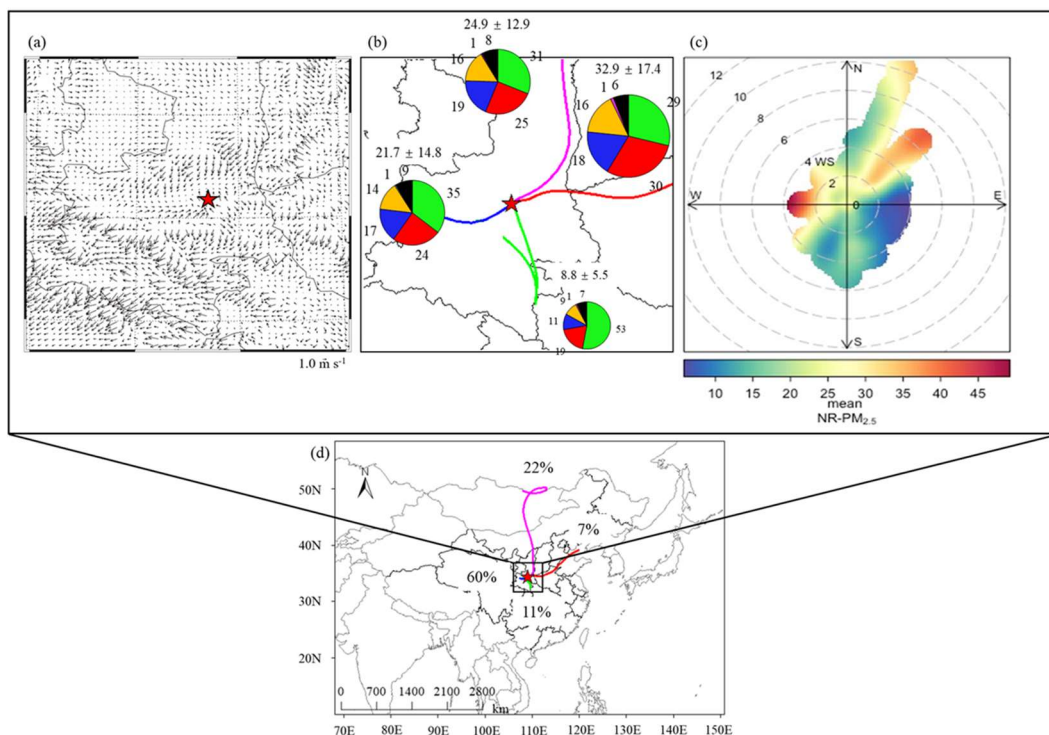
606 Zhong, H., Huang, R., Duan, J., Lin, C., Gu, Y., Wang, Y., Li, Y., Zheng, Y., Chen, Q., Chen, Y.,
607 Dai, W., Ni, H., Chang, Y., Worsnop, D., Xu, W., Ovadnevaite, J., Ceburnis, D., O’Dowd, C.:
608 Seasonal variations in the sources of organic aerosol in Xi’an, Northwest China: the
609 importance of biomass burning and secondary formation. *Sci. Total. Environ.* 737, 139666,
610 2020.

611 Zhong, H., Huang, R., Lin, C., Xu, W., Duan, J., Gu, Y., Huang, W., Ni, H., Zhu, C., You, Y.,
612 Wu, Y., Zhang, R., Ovadnevaite, J., Ceburnis, D., O’Dowd, C.D.: Data for “Measurement
613 report: On the contribution of long-distance transport to the secondary aerosol formation and
614 aging”, Zenodo [data set], <https://doi.org/10.5281/zenodo.6446514>, 2022.



615

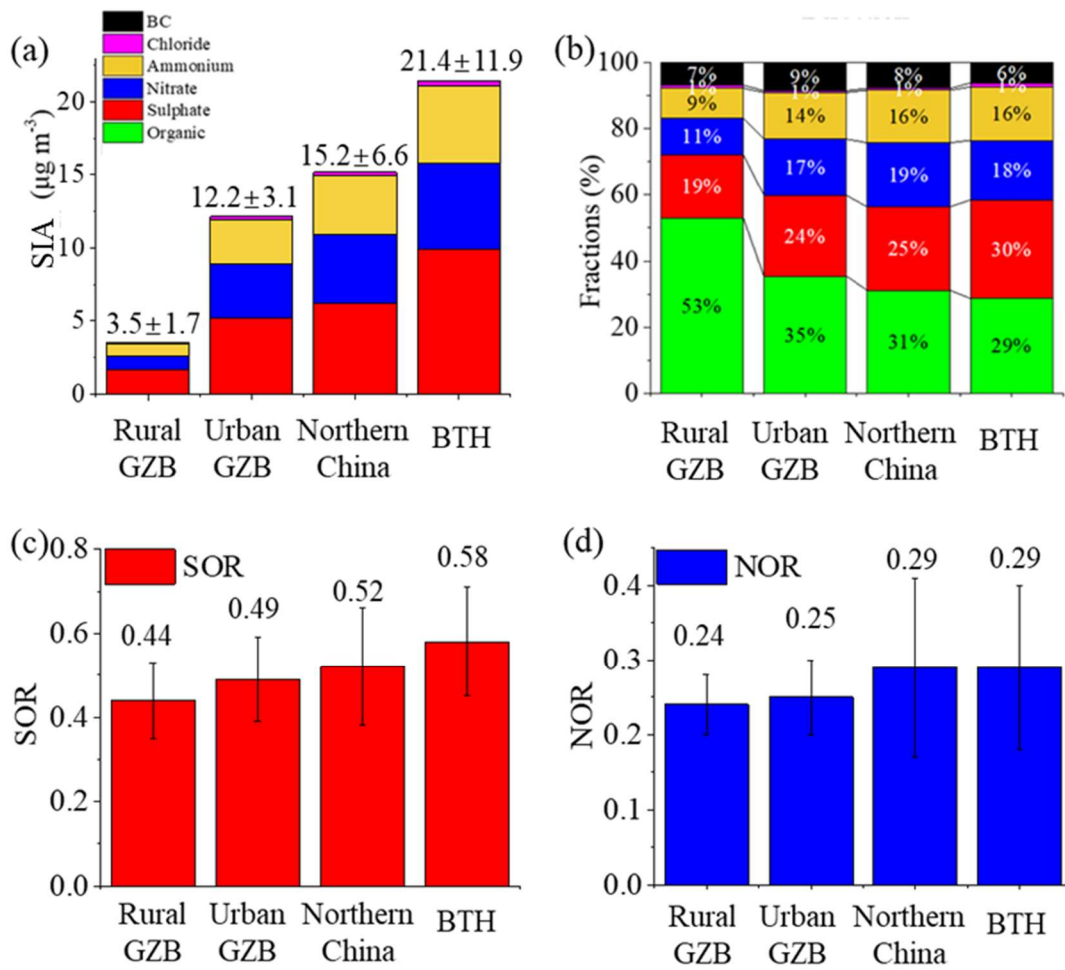
616 **Figure 1.** Time series of (a) relative humidity and temperature, (b, c) mass concentration of
 617 SO₂, CO, NO₂ and O₃ (d, e) mass concentrations and fractional contributions of PM_{2.5} (organics,
 618 sulphate, nitrate, ammonium, chloride and BC) during the campaign period. Five pollution
 619 episodes are observed during the entire campaign, and they are detailed analyzed by HYSPLIT
 620 model and showed in Fig. S3. EP1 and EP2 (shaded) are the only two pollution episodes caused
 621 by continuous transport from the BTH transport and the urban GZB transport, respectively.
 622 Therefore, they are selected for further discussion.



623

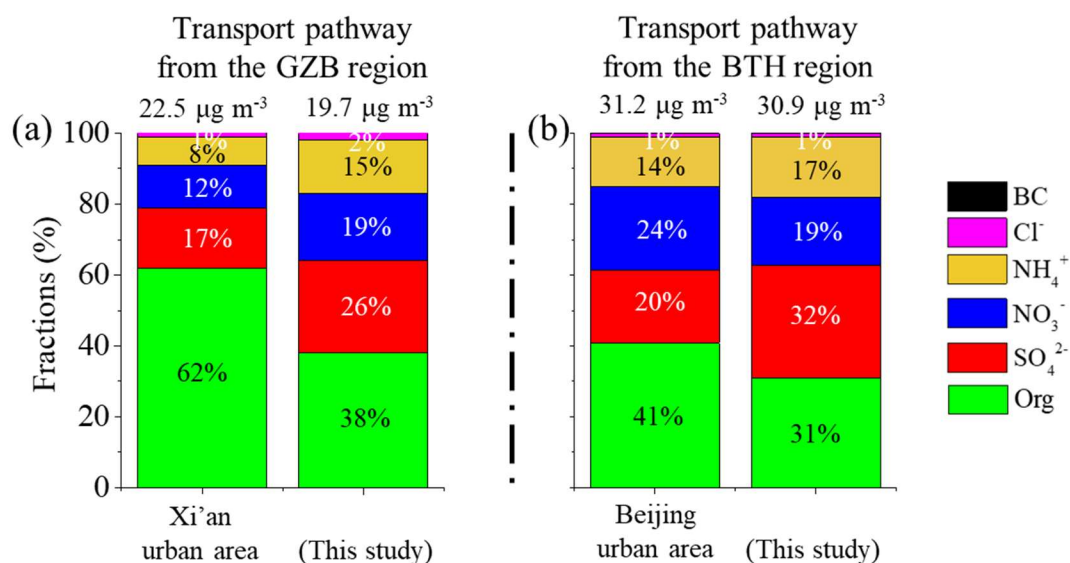
624 **Figure 2.** (a) Wind field, (b, d) backward trajectory and (c) wind rose results during the campaign.
 625 There are four transport clusters observed during the campaign, which are the northern China
 626 transport (the north cluster, magenta, 22% of observing days) and the BTH transport (the east
 627 cluster, red, 7% of observing days), the western GZB transport (the west cluster, blue, 60% of
 628 observing days) and the southern GZB transport (the south cluster, green, 11% of observing days).

629



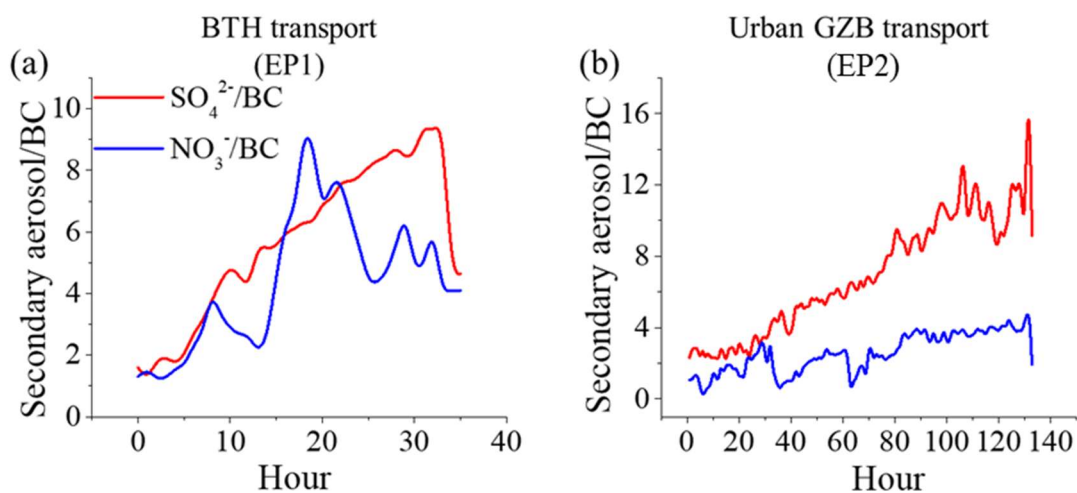
630

631 **Figure 3.** The comparison of (a) the mass concentration of SIA, (b) chemical fractions of $\text{PM}_{2.5}$,
 632 (c) sulphur oxidation ratio (SOR) and (d) nitrogen oxidation ratio (NOR) in four transport
 633 sectors.



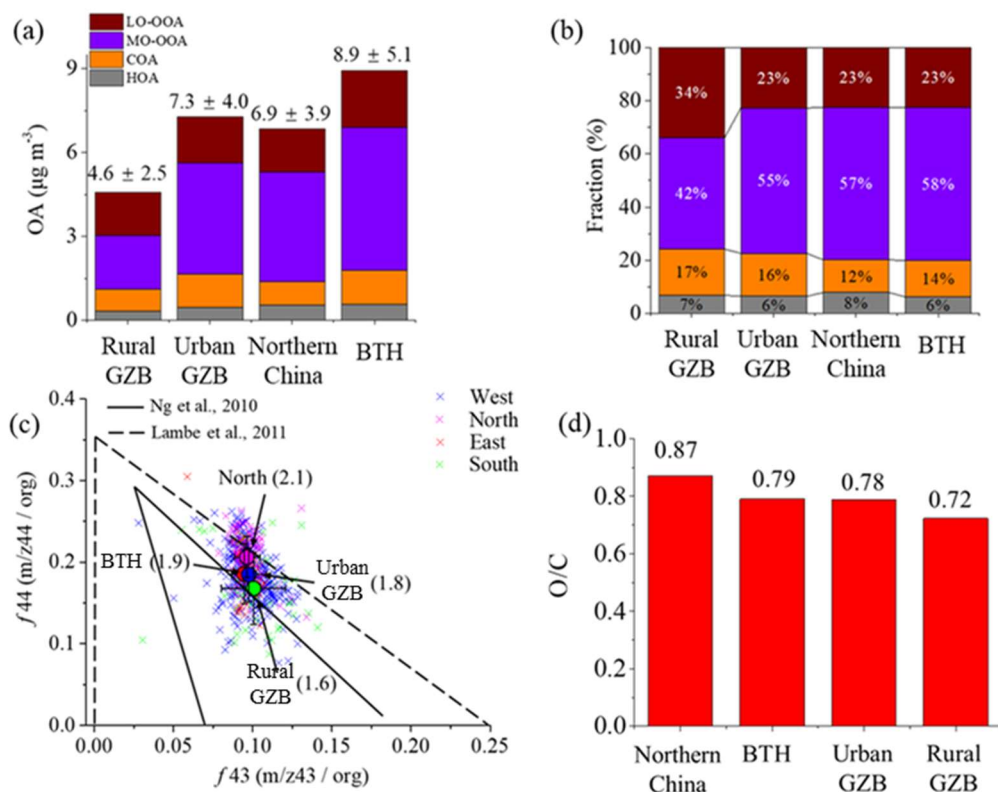
634

635 **Figure 4.** Chemical composition of the observing results which were long-term observation and
 636 were right on the transport route of the BTH transport and the GZB transport, including the
 637 Beijing urban area (Xu et al., 2019), the Xi'an urban area (Duan et al., 20202021), the BTH
 638 transport in this study (East transport) and the urban GZB transport in this study (West
 639 transport).



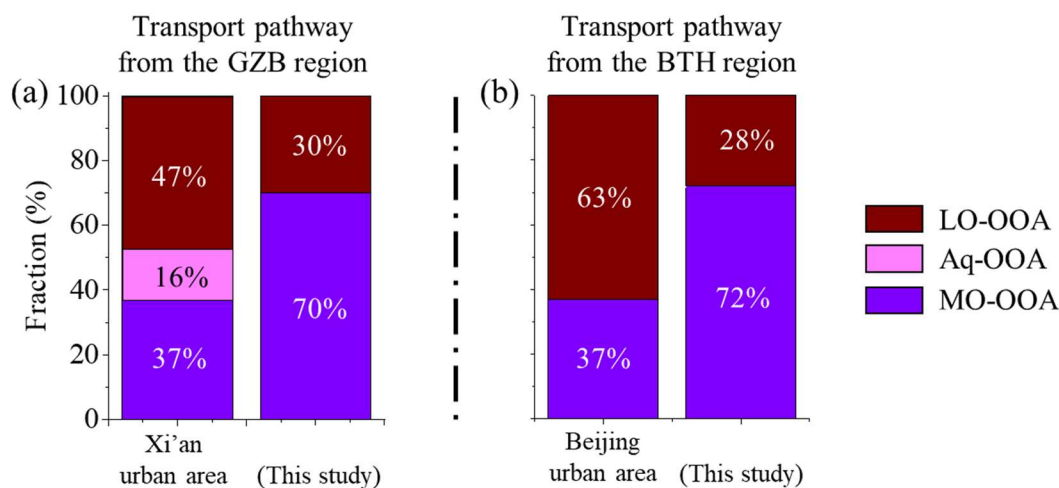
640

641 **Figure 5.** The relationship between production of the secondary inorganic aerosol and transport
 642 duration in the pollution episodes. EP1 and EP2 represented the pollution episodes caused by
 643 the BTH transport and the urban GZB transport, respectively.



644

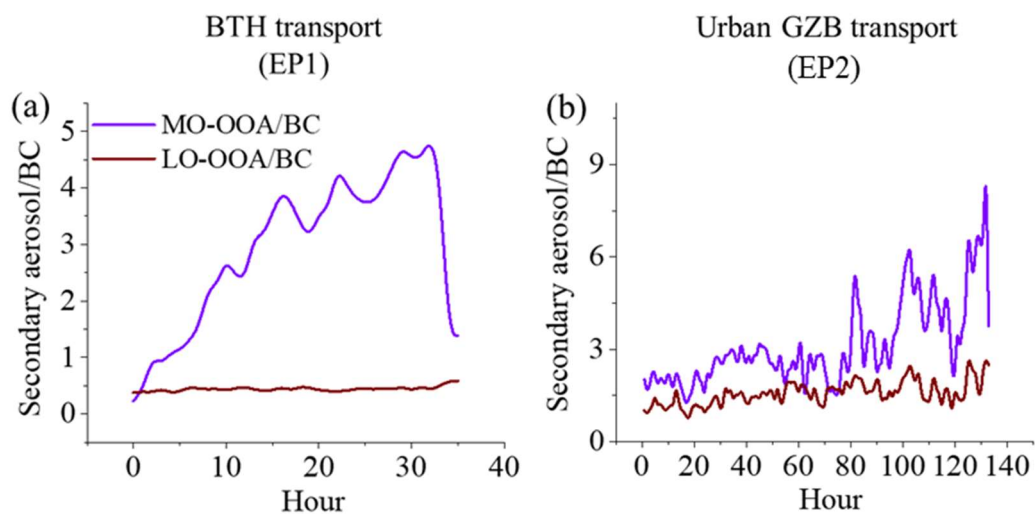
645 **Figure 6.** The comparison of (a) the mass concentration and (b) fractions of organic aerosol. (c)
 646 Scatter plot of f_{44} v.s. f_{43} in four transport directions. The triangle from Ng et al., (2010) and
 647 Lambe et al., (2011) is drawn in solid line and dotted line, respectively. (d) The O/C ratio in four
 648 transport directions.



649

650 **Figure 7.** OA factors of the observing results which were long-term observation and were right
 651 on the transport route of the BTH transport and the GZB transport, including the Beijing urban
 652 area (Xu et al., 2019), the Xi'an urban area (Duan et al., ~~2020~~2021), the BTH transport in this

653 study (East transport) and the urban GZB transport in this study (West transport).



654

655 **Figure 8.** The relationship between production of the secondary organic aerosol and transport
656 duration in the pollution episodes. EP1 and EP2 represented the pollution episodes caused by
657 the BTH transport and the urban GZB transport, respectively.